INTERNATIONAL JOURNAL FOR NUMERICAL METHODS IN FLUIDS, VOL. 2, 317–330 (1982)

NUMERICAL SOLUTION OF SUBSONIC AND TRANSONIC CASCADE FLOWS

W. G. HABASHI*

Concordia University, Montreal, Canada

P. L. KOTIUGA†

Pratt & Whitney Aircraft of Canada Ltd., Longueuil, Quebec, Canada

SUMMARY

In this work a study of the application of the finite element method to transonic flows in axial turbomachines is undertaken.

Solution techniques capable of accurately predicting flows from the incompressible regime up to the establishment of shocks in the transonic regime are presented. In the subsonic and shockless transonic regimes a local linearization method capable of very rapid convergence is used. In the full transonic regime the artificial compressibility method is employed to exclude downstream influences in the supersonic regions. The two approaches can be combined in a unified package and appropriate switches introduced to select the relevant method in any flow regime.

KEY WORDS Transonic flows Turbomachines Finite elements

1. INTRODUCTION

Modern turbomachinery cascade analyses require rapid and accurate numerical solutions, especially in the transonic regime. Cascade codes have traditionally followed the development of corresponding isolated aerofoil algorithms. Type-dependent transonic numerical techniques have enjoyed wide popularity in finite difference methods and have also been applied to the finite volume approach.

A simpler approach, labelled the artificial (AC) compressibility method, has recently been proposed by Eberle.[1] The method consists of modifying the density at supersonic points of the flow, during the solution development, to introduce an artificial viscosity necessary to shock formation. The method is now in wide use for both finite difference and finite element calculations.

2. GOVERNING EQUATIONS AND BOUNDARY CONDITIONS

For the steady, two-dimensional, inviscid, compressible flow of a fluid in a cascade, one can write in terms of the velocity potential

$$\frac{\partial}{\partial x}\left(\frac{\rho b}{\rho_0}\frac{\partial \Phi}{\partial x}\right)+\frac{\partial}{\partial y}\left(\frac{\rho b}{\rho_0}\frac{\partial \Phi}{\partial y}\right)=0 \tag{1}$$

where ρ, ρ_0 and b are density, stagnation density and streamtube depth, respectively.

* Associate Professor. Also Aerodynamics Consultant, Pratt & Whitney Aircraft of Canada Ltd.
† Aerodynamics Engineer.

0271–2091/82/040317–14$01.40
© 1982 by John Wiley & Sons, Ltd.
Received 6 August 1981
Revised 21 December 1981

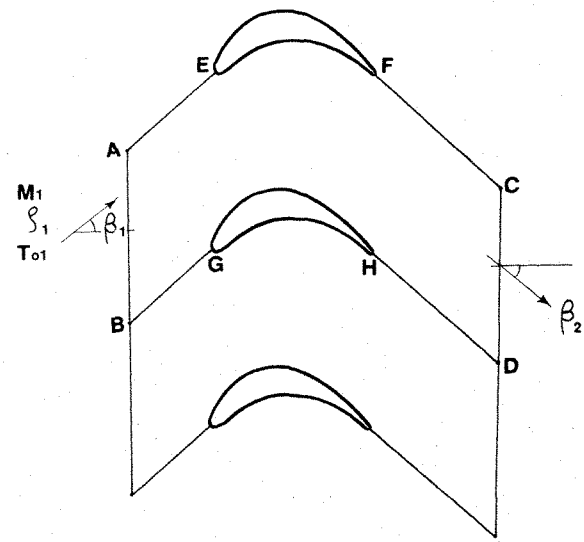

Figure 1. Cascade numerical solution domain

Figure 1 is a sketch of the computational domain adopted. The appropriate boundary conditions become:

$$\text{on } AB \div \frac{\partial \Phi}{\partial n} = a_0[M \cos \beta]_{\text{in}}, \quad \text{i.e. only the axial speed is specified} \tag{2a}$$

$$\text{on } CD \div \frac{\partial \Phi}{\partial n} = a_0[M \cos \beta]_{\text{ex}}, \quad \text{i.e. only the axial speed is specified.} \tag{2b}$$

$$\text{on } AE \div \Phi(x) = \Phi_1(x) + a_0[rsM \sin \beta]_{\text{in}}, \quad \text{a periodicity condition} \tag{2c}$$

where Φ_1 is the potential at the corresponding x point on BG

$$\text{on } FC \div \Phi(x) = \Phi_2(x) + a_0[rsM \sin \beta]_{\text{ex}}, \quad \text{a periodicity condition} \tag{2d}$$

where Φ_2 is the potential at the corresponding x point on HD.

$$\text{on } EF,\ GH \div \text{The no-penetration condition } (\partial\Phi/\partial n = 0) \text{ is enforced} \tag{2e}$$

where n is the outward normal direction to the blade surface at any point, r is the streamtube radius, s is the pitch, M the Mach number and β is the flow angle.
Alternatively, if one selects a stream function formulation, the governing equation becomes:

$$\frac{\partial}{\partial x}\left(\frac{\rho_0}{\rho b}\frac{\partial \psi}{\partial x}\right) + \frac{\partial}{\partial y}\left(\frac{\rho_0}{\rho b}\frac{\partial \psi}{\partial y}\right) = 0 \tag{3}$$

The equation is usually normalized by defining:

$$\frac{\partial \psi}{\partial x} = -\frac{\rho b}{\dot{m}} v; \quad \frac{\partial \psi}{\partial y} = \frac{\rho b}{\dot{m}} u \tag{4}$$

where $\dot{m}$ is the streamtube mass flow rate.

The boundary conditions in this case become:

$$\text{on } AB \div \psi = y/rs \tag{5a}$$

on $CD \div$ again only the axial speed is specified, giving in conjunction with mass continuity

$$\left(\frac{\rho}{\rho_0}\frac{M\cos\beta}{br}\right)_{ex} = \left(\frac{\rho}{\rho_0}\frac{M\cos\beta}{br}\right)_{in} \tag{5b}$$

$$\text{on } BG \div \psi = \psi_1(x); \quad \text{unknown} \tag{5c}$$

$$\text{on } HD \div \psi = \psi_2(x); \quad \text{unknown} \tag{5d}$$

AE and BG are periodic boundaries along which

$$\text{on } AE \div \psi(x) = \psi_1(x) + 1 \tag{5e}$$

$$\text{on } FC \div \psi(x) = \psi_2(x) + 1 \tag{5f}$$

$$\text{on } GH \div \psi = 0$$

$$\text{on } EF \div \psi = 1$$

The governing equation (1) or its alternative form of equation (3) are complemented by the isentropic relationship

$$\frac{\rho}{\rho_0} = \left[1 - \frac{\gamma - 1}{2} M_0^2\right]^{1/\gamma - 1} \tag{6}$$

where γ is the isentropic exponent.

3. SUBSONIC SOLUTIONS

For the subsonic regime, the governing equation is elliptic and to speed up convergence we adopt a local linearization scheme appropriate to finite elements.[2,3] If an initial solution can be determined at a low Mach number, one can assume the solution at a slightly higher Mach number to be a small perturbation around it. Our initial solution is normally the incompressible one obtained by setting $\rho = \rho_0$ everywhere, for equations (1) or (3). Then by determining, in each element, a local velocity direction ξ_e and a normal to it η_e, say at the centroid, one can assume

$$\psi_e^{(n+1)} = \frac{b\rho_e^{(n)} V_e^{(n)} \eta_e}{\dot{m}} + \psi'(\xi_e, \eta_e) \tag{7}$$

where ψ' is a stream function defining the perturbation velocity components

$$V_e^{(n+1)} = [V_e^{(n)} + u'; v'] \tag{8}$$

$$\frac{u'}{V_e^{(n)}}, \frac{v'}{V_e^{(n)}} \ll 1$$

The perturbation stream function (ψ') can be shown to satisfy the Prandtl–Glauert equation

$$\frac{1}{\rho_e b}\left[(1 - M_e^2)\frac{\partial^2 \psi'}{\partial \xi_e^2} + \frac{\partial^2 \psi'}{\partial \eta_e^2}\right] = 0 \tag{9}$$

within each element. An appropriate variational integral for (9) is

$$I^e(\psi') = \frac{1}{2\rho_e b} \iint_{A_e} \{(1-M_e^2)\psi_{\xi_e}^2 + \psi_{\eta_e}^2\} \, d\xi_e \, d\eta_e - \oint_{C_e} \frac{1}{\rho_e b} \psi' \left(\frac{\partial \psi'}{\partial n_e}\right) ds_e \tag{10}$$

Equation (10) is then rewritten in terms of the global stream function (ψ) and one obtains, after the cancellation of the contour integral term over adjacent inner element boundaries:

$$I(\psi) = \sum_{e=1}^{N} \frac{1}{2\rho_e b} \iint_{A_e} [(1-M_e^2)\psi_{\xi_e}^2 + \psi_{\eta_e}^2] \, d\xi_e \, d\eta_e - \oint_C \frac{1}{\rho b} \psi \left(\frac{\partial \psi}{\partial n}\right) ds \tag{11a}$$

where C is the outer contour of the calculation domain and N the total number of elements in the domain.

A similar procedure can be applied to equation (1) resulting in the variational integral:[3]

$$I(\Phi) = \sum_{e=1}^{N} \frac{\rho_e b}{2} \iint_{A_e} [(1-M_e^2)\Phi_{\xi_e}^2 + \Phi_{\eta_e}^2 + 2V_e M_e^2 \Phi_{\xi_e}] \, d\xi_e \, d\eta_e - \oint_C \rho b \Phi \left(\frac{\partial \Phi}{\partial n}\right) ds \tag{11b}$$

Equation (11a), or alternatively equation (11b), provides an iterative procedure that takes into consideration the physics of the flow. The change in the type of governing equation at transonic speeds shows up naturally in the integral and contributes greatly to rapid convergence at these speeds.

4. TRANSONIC SOLUTIONS

For the transonic regime the proper influences have to be accounted for and downstream influences excluded at supersonic points. While finite difference relaxation schemes are highly developed for this problem, finite element methods have proved difficult and cumbersome for transonic flows. Recently, however, Eberle[1] and Hafez *et al.*[4] have developed the artificial compressibility method for finite elements and for finite differences, respectively. By replacing the density ρ at supersonic points by an artificial density $\tilde{\rho}$ calculated at a point slightly upstream, an artificial viscosity is introduced into equation (1), and shock waves evolve naturally in the solution of transonic flows. It is not clear in Eberle's work exactly where to take the artificial density $\tilde{\rho}$. Hafez *et al.*'s scheme, however, is systematic and assigns at any supersonic point P the density $\tilde{\rho}$ such that:

$$\tilde{\rho} = \rho - \mu \left(\frac{\partial \rho}{\partial s}\right) \Delta s \tag{12}$$

where

$$\frac{\partial \rho}{\partial s} \Delta s \simeq \frac{u}{V} \left(\frac{\partial \rho}{\partial x}\right) \Delta x + \frac{v}{V} \left(\frac{\partial \rho}{\partial y}\right) \Delta y \tag{12a}$$

μ being the coefficient of artificial compressibility and s the streamline direction.

If, in a finite element solution, the grid is aligned approximately with the streamlines one

can safely adopt Hafez *et al.*'s approach of calculating the artificial density using the density gradient between the centroids of adjacent elements.

5. FINITE ELEMENT DISCRETIZATION

Within each element

$$\psi(x, y) = \sum_{i=1}^{n} N_i(\xi, \eta)\psi_i \tag{13}$$

where in the present work n has been taken as 3, 4 or 8, i.e. for simple constant derivative triangular elements or isoparametric 4- and 8-node quadrilaterals. Upon minimization we obtain at the element level, for the stream function formulation

$$[k]^{(e)}\{\psi\}^{(e)} = \{R\}^{(e)} \tag{14}$$

$$k_{ij} = \iint_{A_e} \frac{1}{\rho_e b}\left[(1-M_e^2)\frac{\partial N_i}{\partial \xi_e}\frac{\partial N_j}{\partial \xi_e} + \frac{\partial N_i}{\partial \eta_e}\frac{\partial N_j}{\partial \eta_e}\right] d\xi_e\, d\eta_e \tag{14a}$$

$R_i = \oint \frac{N_i}{\rho_e b}\left(\frac{\partial \psi}{\partial n}\right) ds$, for elements having a boundary on AB or CD, i.e.

$$R_i = \left[\frac{\rho_0}{\rho_{ex}}\frac{\tan \beta_{ex}}{s} + \frac{\rho_0}{\rho_{in}}\frac{\tan \beta_{in}}{s}\right] \int_0^s N_i\, d\theta \tag{15}$$

where R is the right-hand side. The explicit form of the shape functions $N_i(\xi, \eta)$ can be found in any finite element reference (such as Reference 5). In the isoparametric approach the element edges' geometry is described by the same approximation function as equation (13):

$$x = \sum_{i=1}^{n} N_i(\xi, \eta)x_i \tag{16a}$$

and

$$y = \sum_{i=1}^{n} N_i(\xi, \eta)y_i \tag{16b}$$

Since $dy = r\, d\theta$ we prefer to replace (16b) by

$$\theta = \sum_{i=1}^{n} N_i(\xi, \eta)\theta_i \tag{16c}$$

Since all shape functions N_i are in terms of the local co-ordinates (ξ, η) one proceeds as follows:

$$\begin{Bmatrix} \frac{\partial N_i}{\partial \xi} \\ \frac{\partial N_i}{\partial \eta} \end{Bmatrix} = \begin{bmatrix} \frac{\partial x}{\partial \xi} & \frac{\partial \theta}{\partial \xi} \\ \frac{\partial x}{\partial \eta} & \frac{\partial \theta}{\partial \eta} \end{bmatrix} \begin{Bmatrix} \frac{\partial N_i}{\partial x} \\ \frac{\partial N_i}{\partial \theta} \end{Bmatrix} \tag{17}$$

or inverting the Jacobian of the transformation

$$\begin{Bmatrix} \frac{\partial N_i}{\partial x} \\ \frac{\partial N_i}{\partial \theta} \end{Bmatrix} = [J]^{-1} \begin{Bmatrix} \frac{\partial N_i}{\partial \xi} \\ \frac{\partial N_i}{\partial \eta} \end{Bmatrix} \tag{18}$$

where $[J]$ and $[J]^{-1}$ can be explicitly calculated for each element. A further transformation is needed to obtain the shape function derivatives with respect to the local flow direction in each element

$$\begin{Bmatrix} \dfrac{\partial N_i}{\partial \xi_e} \\ \dfrac{\partial N_i}{\partial \eta_e} \end{Bmatrix} = \begin{bmatrix} \cos\sigma & \sin\sigma \\ -\sin\sigma & \cos\sigma \end{bmatrix}^{(e)} \begin{Bmatrix} \dfrac{\partial N_i}{\partial x} \\ \dfrac{\partial N_i}{r\,\mathrm{d}\theta} \end{Bmatrix} \tag{19}$$

where the flow angle $\sigma^{(e)}$ is updated during each iteration as:

$$\sigma^{(e)} = \tan^{-1}\left(\frac{\dfrac{-\partial\psi}{\partial x}}{\dfrac{\partial\psi}{\partial y}}\right)^{(e)} = \tan^{-1}\left(\frac{\left[\dfrac{\partial N_i}{\partial x}\right]\{\psi_i\}}{\dfrac{1}{r}\left[\dfrac{\partial N_i}{\partial\theta}\right]\{\psi_i\}}\right)^{(e)} \tag{20}$$

Only one flow angle σ is calculated at the centroid for the case of triangular or quadrilateral elements. After substituting (19) into (14a), the influence matrix is formed for each element by a 3×3 Gaussian integration and assembled in the usual fashion to yield

$$[K]\{\psi\} = \{R\} \tag{21}$$

The variational integral is identical in the transonic case with $M_e = 0$ in equation (14). Only 4-node quadrilateral elements have been used for transonic solutions.

6. DOMAIN DISCRETIZATION

The construction of appropriate computational grids for cascades is always a challenging problem. In an industrial situation where such an analysis program would be used in a 'black-box' form, any mesh generation scheme should be fully automated. Several solution schemes have been presented in the literature and use different methods for the generation of such grids.[6–8] Finite difference schemes usually require the mapping of the computational domain into a rectangular region whereas finite area schemes[7] require the centring of control volumes, around each nodal point, across which continuity of flow variables is imposed.

In the present work we start by splining the co-ordinates of the blade. Local splines are found necessary for high turning turbine blades. Leading and trailing edge circles are then fitted at both ends of compressor blades. Several element layers resembling the blade shape could be added. The remainder of the grid is generated isoparametrically between the last element layers (Figure 2). Upstream and downstream sections are also constructed in an expanding fashion. For the case of 8-node isoparametric elements, the location of the exact

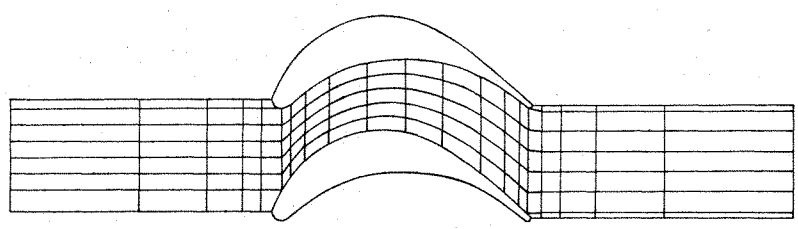

Figure 2. Finite element automatically generated grid

mid-points is an important factor in the solution but has received scant attention in the literature. On the blade, for example, one proceeds by connecting the two corner nodes of each element by a straight line. By constructing a normal to this line, at its mid-point, and finding the intersection of this normal with the spline describing the blade, one would have located the exact mid-point of the parabola that replaces the spline in the analysis. If the analysis is for triangular elements, the same grid is used and each parabolic element broken internally into 6 triangular elements.

7. FEATURES OF THE SOLUTION

The program tested contained the following options that could be specified interactively by the user:

(a) Stream Function Solution.
(b) Velocity Potential Solution.
(c) Local-linearization.
(d) Triangular, 4-node and 8-node quadrilateral elements.
(e) Arbitrary radius and height of the axisymmetric streamtube analysed in the blade-to-blade plane.
(f) Complete freedom in specification of number of points and their distribution on the blade, across the pitch and in the upstream/downstream sections. The inlet/exit sections are built in an expanding fashion and can also be slanted to match the flow angles.

During each iteration, the matrix $[K]$ of equation (21) is assembled in the 'Skyline' form described in Reference 5. Essentially the element topology is first scanned and the bandwidth of each row predetermined. The variable bandwidth matrix $[K]$ is then stored in vector form, with a vector of pointers to the addresses of diagonal elements. The scheme is efficient, especially if element layers are generated around the blade and the bandwidth of only a few rows increases substantially.

The symmetric matrix is solved by LL^T decomposition using the program described in the previous reference. Convergence to an accuracy of 0·01 per cent in the density for subsonic flows occurs in about 4 to 6 iterations and global solution times are below 7 sec on a Cyber 175 computer.

An important comment to be added concerns the extraction of Mach numbers from the ψ or Φ solution. Although for 8-node isoparametric elements the Mach number distribution is linear within an element, it is discontinuous across the elements. Hinton *et al.*'s method[9] has proven innately accurate in obtaining corner values of the Mach number from the precise values obtainable at the Gaussian points. Large non-physical velocity peaks would usually result at leading and trailing edges without the use of this method.

For the artificial compressibility method we use the locally linearized approach during 3 or 4 iterations to provide an initial good guess to the transonic solution. Afterwards a successive line overrelaxation method is used to implement the AC solution. Two comments are worth making here. First, at each vertical line of the inlet/exit sections, a periodicity condition must be enforced. For the symmetric test case presented here (Figure 11), the periodicity constant is zero. However, to enable the use of a tridiagonal solver one can, for example, assume all points on AE (Figure 1) to be known, with periodicity respected, from the previous iteration. Solution symmetry, however, is immediately destroyed and one needs to repeat the line

relaxation procedure several times at the same station to recover symmetry. The physical explanation is simple since such an approach is equivalent to specifying nodal values on AE while imposing a condition $\partial\Phi/\partial n = 0$ on BG during the solution. If one chooses implicitly to account for periodicity at each line, the tridiagonal structure is destroyed. Using the skyline method, however, the matrix size at each line is limited and solution times are unaffected. The same solver is then used for subsonic and transonic solutions.

Secondly, it is imperative to update the last station in the cascade since no ϕ values are specified on this line. We solve for the last station, and the line preceding it, simultaneously during each field sweep. This has the minor effect of increasing the matrix skyline only when the last station is reached.

8. TEST CASES AND RESULTS

Several test cases are presented here. The method's accuracy has been verified against analytical, experimental and other numerical data. In Figure 3 our stream function solution is compared to the incompressible analytical solution of Gostelow and Smith.[10] All other cases presented use the velocity potential approach.

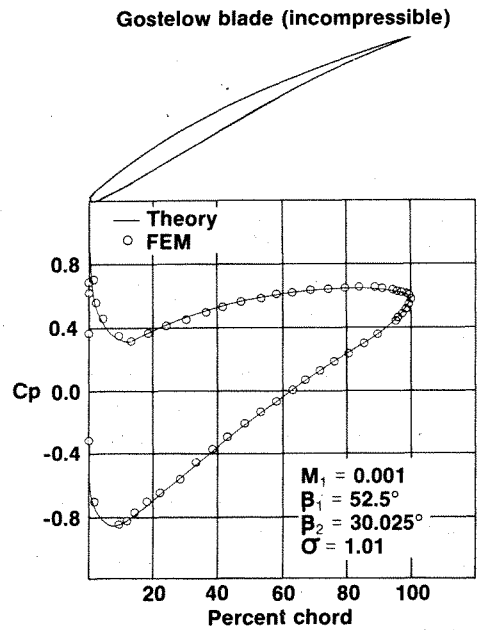

Figure 3. Incompressible flow over Gostelow cascade using stream function formulation, 8-node element

In Figure 4 an impulse turbine cascade, designed by Stanitz and Sheldrake,[11] is successfully analysed and the solution compares well against the experimentally available data.

Figures 5 and 6 compare the solutions for a flow over a compressor blade designed by Stanitz and Sheldrake's hodograph method,[11] using triangular and 8-node isoparametric elements. The superiority of the latter element is evident. Figure 6 also shows the 8-node

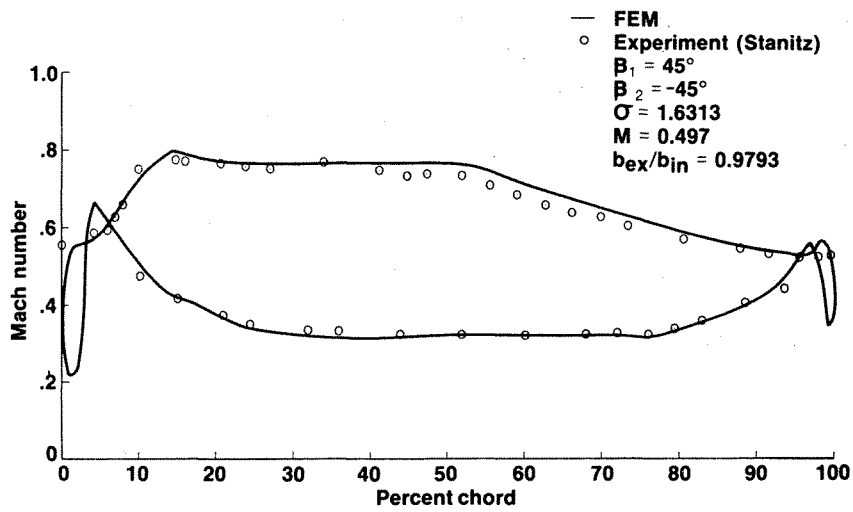

Figure 4. Stanitz impulse turbine blade, potential formulation, 8-node element

element solution to the same blade but on an arbitrary surface described by

x	r	b	A/A_{LE}
−2·5523	6·6231	1·0191	0·94465
0·0	7·1454	1·000	1·000
0·952	6·9550	1·0006	0·88323
1·904	6·7625	0·97235	0·92024

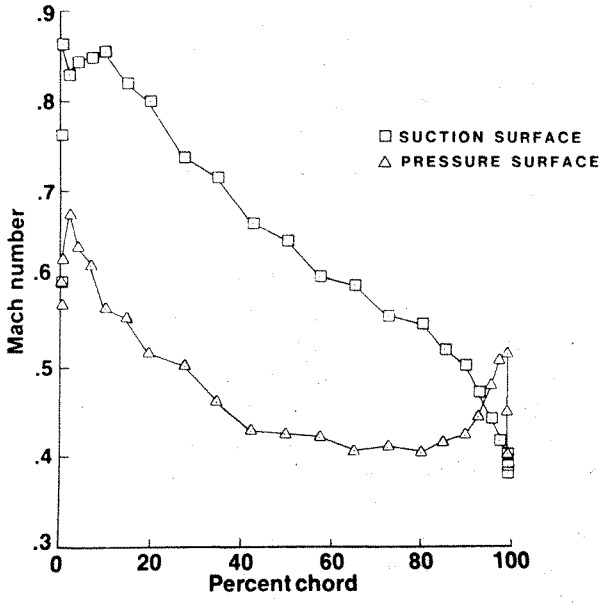

Figure 5. Hodograph designed blade, potential formulation, triangular element

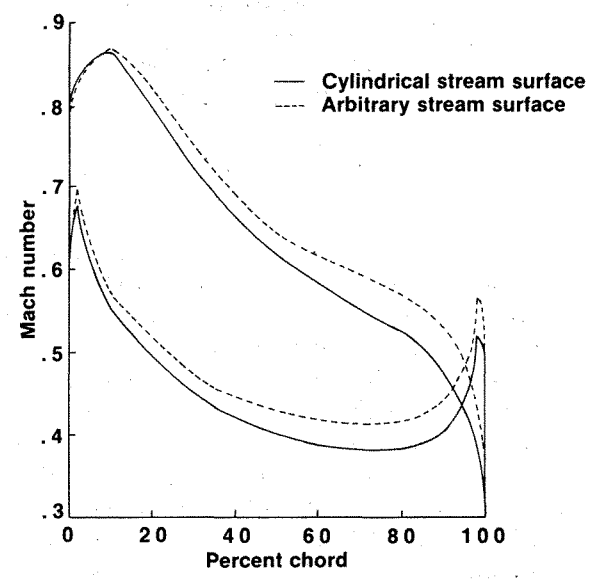

Figure 6. Hodograph designed blade, potential formulation, 8-node element

More points are used to describe this surface in the actual solution and r and b become additional variables in the Gaussian integration of each element. Although no experimental or other numerical data are available for comparison in this case, we estimate accuracy by integrating the torque profile around the blade and comparing against the imposed angular momentum change between inlet and exit. The error is less than 0·2 per cent.

Two shockless transonic turbine blades (Figures 7 and 8) designed by Hobson[12] are also compared with the numerical predictions by this FEM code using the 8-node element. Despite not accurately predicting the peak (Figure 7), both results are in good agreement with the hodograph design.

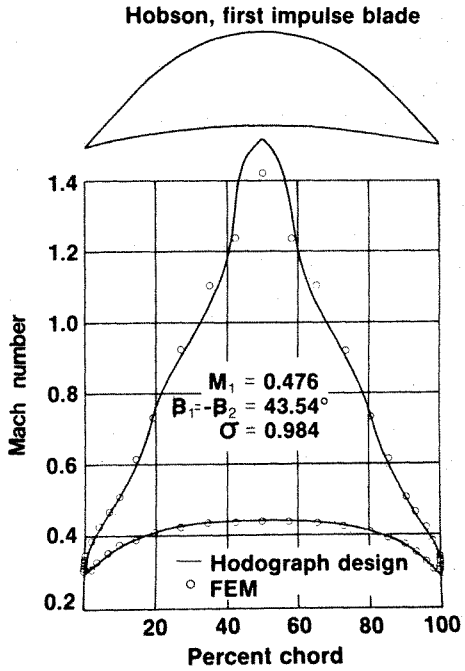

Figure 7. Hobson first impulse shockless transonic blade, potential formulation, 8-node element

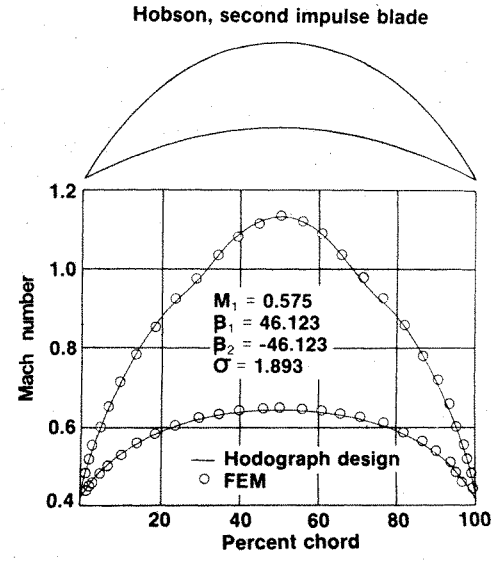

Figure 8. Hobson second impulse shockless transonic blade, potential formulation, 8-node element

Figures 9 and 10 show the comparisons of flow results over a shockless transonic compressor blade designed by Korn[7] using the subsonic 8-node element solver and also the artificial compressibility method using bilinear elements. We conclude, from our experience, that local linearization is twice as fast as no linearization for the same final accuracy.

Other results have also been obtained using the artificial compressibility method and bilinear elements. Figure 11 demonstrates the shock capturing capability of the AC method for the flow over a non-staggered cascade of NACA 0012 aerofoils at $M = 0{\cdot}77$; we note in these diagrams the perfect symmetry of the pressure and suction surface distributions. The results compare well with the transonic small disturbance results obtainable with the method of Jones and Dickinson.[13] Figure 12 represents the prediction for a 6 per cent parabolic arc isolated aerofoil solved for in a low-solidity cascade form at $M = 0{\cdot}9$ compared with Jones and Dickinson's[13] results. Finally, Figures 13(a) and (b) show the calculated Mach numbers and contours over a staggered transonic compressor blade row.

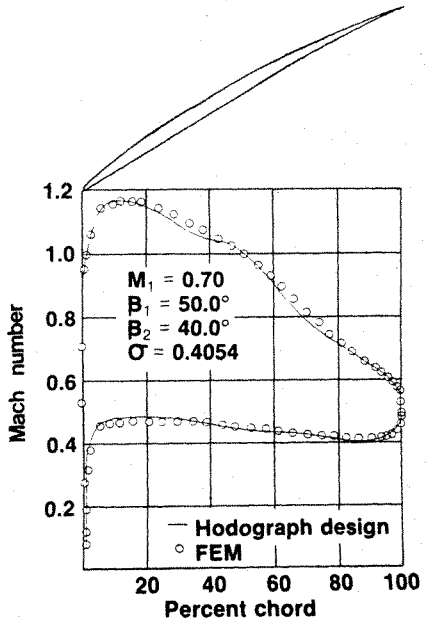

Figure 9. Korn shockless transonic blade, potential formulation, 8-node element with local linearization

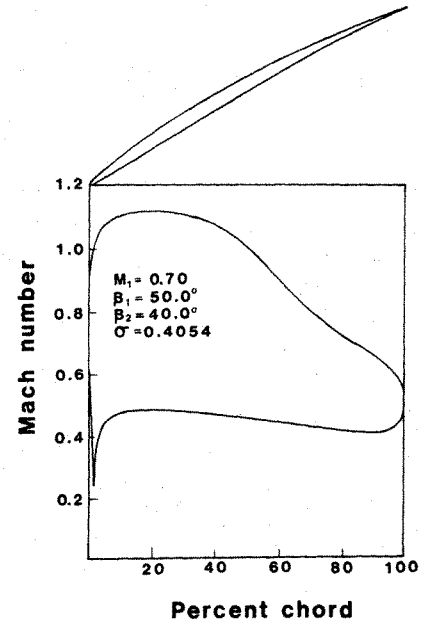

Fig. 10. Korn shockless transonic blade, potential formulation, bilinear element with artificial compressibility

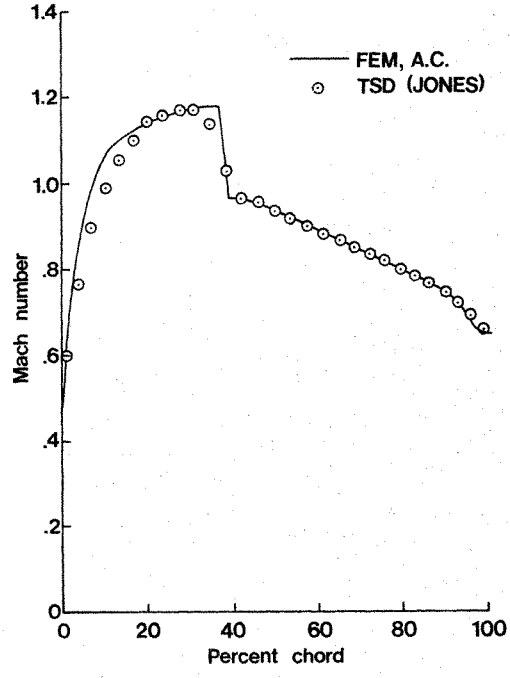

Figure 11. NACA 0012 unstaggered cascade, $M = 0{\cdot}77$, potential formulation, bilinear element with artificial compressibility

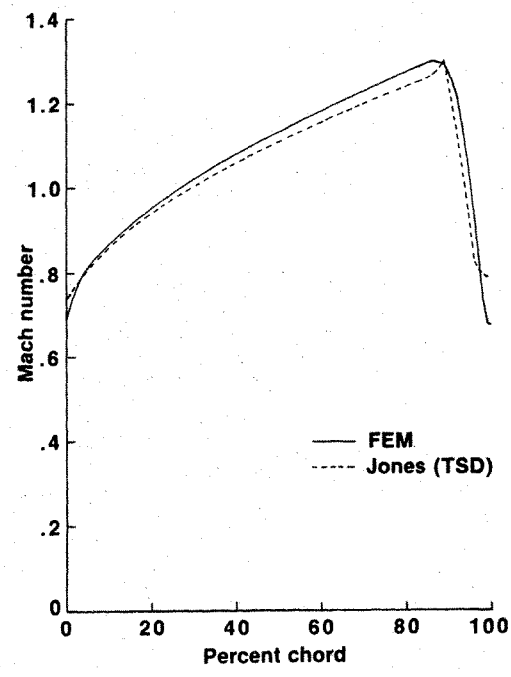

Figure 12. 6 per cent parabolic arc unstaggered cascade, $M = 0{\cdot}90$, potential formulation, bilinear element with artificial compressibility

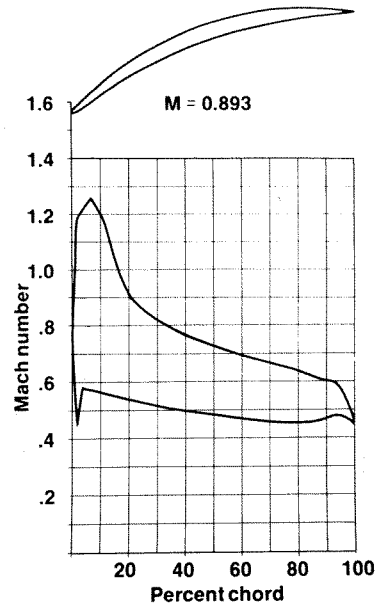

Figure 13(a). Multiple circular arcs cascade, $M = 0{\cdot}90$, potential formulation bilinear element with artificial compressibility

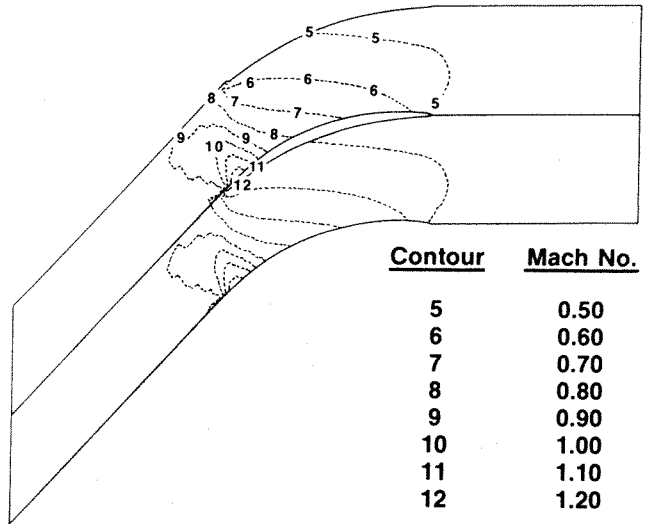

Figure 13(b). Mach number contours for cascade of Figure 13(a)

9. CONCLUSIONS

A versatile and accurate finite element method is presented for the solution of transonic cascades. Test cases compare favourably with theory experiments and hodograph designs in

both the subsonic and transonic regimes. Solution times for the subsonic cases are very short (7 sec), whereas those for transonic solutions with shocks are of the order of 100 to 200 sec on a Cyber 175 computer.

ACKNOWLEDGEMENTS

This work has been partially supported by grants A–3662 and PRAI–7901 of the Natural Sciences and Engineering Research Council of Canada (NSERC).

The authors would like to acknowledge the many challenging and fruitful discussions they had with Dr. Denis J. Jones of NSERC.

APPENDIX

Nomenclature

a	speed of sound
A	cross-sectional area of streamtube
AC	artificial compressibility
b	streamtube depth
C	outer contour of solution domain
FEM	Finite element method
I	variational integral
J	Jacobian of the transformation
k	element influence matrix
K	global influence matrix
M	Mach number
$\dot{m}$	streamtube mass flow rate per blade passage
n	outward normal direction to the solution domain boundary
N_i	shape function
r	radius of streamtube
R	right-hand side of finite element matrix equation
s	pitch in radians, 2π/(number of blades); also streamline direction
TSD	transonic small disturbance solutions
u, v	velocity components in x and y directions, respectively
V	meridional flow
x, y	meridional distance; tangential distance
β	flow angle far upstream and downstream
γ	isentropic exponent
θ	circumferential distance measured from bottom left of selected solution domain (Figure 1), $y = r\theta$
ξ, η	local normalized co-ordinates within elements
ξ_e, η_e	local velocity direction in element e and its normal respectively.
ρ	density
$\tilde{\rho}$	artificial density
σ	velocity direction in an element with respect to x axis; also solidity
ψ	stream function
ϕ, Φ	velocity potential

μ artificial compressibility coefficient
[ ] matrix
{ } vector
[ ] transpose of a vector

Subscripts

i property at nodal point i
0 stagnation property
∞ conditions far upstream
(in) property at channel inlet
(ex) property at channel exit
(e) property of element e

REFERENCES

1. A. Eberle, 'Transonic potential flow computations by finite elements: airfoil and wing analysis, airfoil optimization', Messerschmidt-Böllkow-Blohm GBH, UF 1428 (ö), 1978.
2. S. F. Shen and W. G. Habashi, 'Local linearization of the finite element method and its applications to compressible flows, *Int j. numer. methods eng.*, **10,** 565–577 (1976).
3. W. G. Habashi, E. G. Dueck and D. P. Kenny, 'Finite-element approach to compressor blade-to-blade cascade analysis', *AIAA J.*, **17,** 693–698 (1979).
4. M. M. Hafez, J. C. South and E. M. Murman, 'Artificial compressibility methods for numerical solution of transonic full potential equations', *AIAA J.*, **17,** 838–844 (1979).
5. K. Bathe and E. L. Wilson, *Numerical Methods in Finite Element Analysis*, Prentice-Hall, 1976.
6. C. Hirsch and G. Warzee, 'Finite element computation of subsonic cascade flows', *Proc. 6th Canadian Cong. Appl. Mech.*, Vancouver, B.C., June (1977).
7. D. C. Ives and F. F. Liutermoza, 'Second-order accurate calculation of transonic flow over turbomachinery cascades', *AIAA J.* **17,** 870–876 (1979).
8. J. R. Caspar, D. E. Hobbs and R. L. Davis, 'Calculation of two-dimensional potential cascade flow using finite area methods', *AIAA J.*, **18,** 103–109 (1980).
9. E. Hinton, F. C. Scott and R. E. Ricketts, 'Local least squares stress smoothing for parabolic isoparametric elements', *Int. j. numer. methods eng.*, **9,** 235–239 (1975).
10. J. P. Gostelow and D. J. L. Smith, 'Test cases for turbomachinery flow field computation', Cambridge University, Engineering Department, *CUED/A/TURBO/TR 48*, June (1973).
11. J. D. Stanitz and L. J. Sheldrake, 'Application of a channel design method to high solidity cascades and tests of an impulse cascade with 90° of turning', *NACA Rept. 1116* (1950).
12. D. G. Hobson, 'Shock-free transonic flow in turbomachinery cascades', *Report CUED/A/TURBO/TR 65*, (1974).
13. D. J. Jones and R. G. Dickinson, 'A description of the NAE two-dimensional transonic small disturbance computer method', National Research Council Canada, *Lab Tech Rept LTR–HA–39*, January (1980).